

A nearly relaxation-free opto-electronic memory from ultra-thin graphene-MoS₂ binary hybrids

Kallol Roy,^{1‡} Medini Padmanabhan,¹ Srijit Goswami,^{1*} T. Phanindra Sai,¹
Gopalakrishnan Ramalingam,^{2†} Srinivasan Raghavan,² and Arindam Ghosh^{1‡}
¹*Department of Physics, Indian Institute of Science, Bangalore 560012, India and*
²*Materials Research Center, Indian Institute of Science, Bangalore 560012, India*

Ultra-thin planar heterostructures of graphene and other two-dimensional crystals have recently attracted much interest. Very high carrier mobility in a graphene-on-boron nitride assembly is now well-established [1, 2], but it has been anticipated that appropriately designed hybrids could perform other tasks as well [3]. A heterostructure of graphene and molybdenum disulphide (MoS₂) is expected to be sensitive to photo illumination due to the optical bandgap in MoS₂ [4]. Despite significant advances in device architectures with both graphene [5–8] and MoS₂ [9–13], binary graphene-MoS₂ hybrids have not been realized so far, and the promising opto-electronic properties of such structures remain elusive. Here we demonstrate experimentally that graphene-on-MoS₂ binary heterostructures display an unexpected and remarkable persistent photoconductivity under illumination of white light. The photoconductivity can not only be tuned independently with both light intensity and back gate voltage, but in response to a suitable combination of light and gate voltage pulses the device functions as a re-writable optoelectronic switch or memory. The persistent, or ‘ON’, state shows virtually no relaxation or decay within the experimental time scales for low and moderate photoexcitation intensity, indicating a near-perfect charge retention. A microscopic model associates the persistence with strong localization of carriers in MoS₂. These effects are also observable at room temperature, and with chemical vapour deposited graphene, and hence are naturally scalable for large area applications.

Many optical switches and memories rely on persistent photoconductivity (PPC) where electromagnetic excitation shifts the electrical resistance of the host material to a slowly relaxing state. Traditionally, PPC is observed in compound semiconductors, alloys and heterojunctions [14–16], but more recently, assemblies of

carbon-based nano-materials [17] have also received considerable interest. External tunability of the PPC, for example with a gate, makes such designs particularly attractive for switching and read-write memory applications, as demonstrated with nanotubes dispersed in photoactive polymers [17].

PPC has so far not been realized in graphene-based field-effect devices, although such devices would readily benefit from strong coupling to light over a wide band of wavelengths in graphene [18, 19], and fast recombination life times [20–23], along with gate-tunability, miniaturization and ability to pattern over a large area [7]. A significant improvement in photoconductivity of graphene has been achieved by combining graphene with other light absorbing materials such as quantum dots [24] and chromophores [25]. This indicates that exotic optoelectronic response could be engineered in graphene-based hybrids with an appropriate choice of complementary materials.

Molybdenum disulphide (MoS₂) is intrinsically responsive to light, owing to its bandgap which increases from about 1.2 eV (indirect) in bulk/multilayer MoS₂ to 1.9 eV (direct) for a single molecular layer [4]. MoS₂ can also be exfoliated mechanically, and can be stabilized in single or multilayered form on insulating substrate [9, 26]. This opens up an avenue to create planar heterojunctions of Graphene and MoS₂ through physical proximity. In this work we have explored the opto-electronic properties of such planar graphene-MoS₂ hybrids.

The device architecture, process flow and measurement layout are shown in Fig. 1a. We have used single layer graphene and multilayer (≈ 10 molecular layers) MoS₂, both of which were obtained via mechanical exfoliation, and subsequently overlaid by vertical alignment (see methods for details). This technique is same as that for overlaying exfoliated graphene on BN microflakes, which provides a trap-free high-quality interface [1, 2], essential for the present experiments. In all devices, the MoS₂ was exfoliated on a SiO₂/p⁺-Si substrate, and graphene was then transferred on top of MoS₂. The layout of the electrical leads can be designed to measure the four-probe resistance (R) of graphene (on MoS₂), and two-probe conductance (G_{MoS_2}) of the underlying MoS₂ (that is not covered by graphene) simultaneously. The devices were loaded on a variable-temperature cryostat along with a commercial white light emitting diode (LED) to provide the photo excitation.

Typical gate voltage (V_g) characteristics, recorded at 110 K, of the graphene (on-MoS₂) and bare MoS₂ re-

*present address: Kavli Institute of Nanoscience, Delft University of Technology, P.O. Box 5046, 2600 GA Delft, The Netherlands.

†present address: Department of Materials Science and Engineering, University of Virginia, Charlottesville 22904, United States.

‡correspondence information: kallol@physics.iisc.ernet.in, arindam@physics.iisc.ernet.in

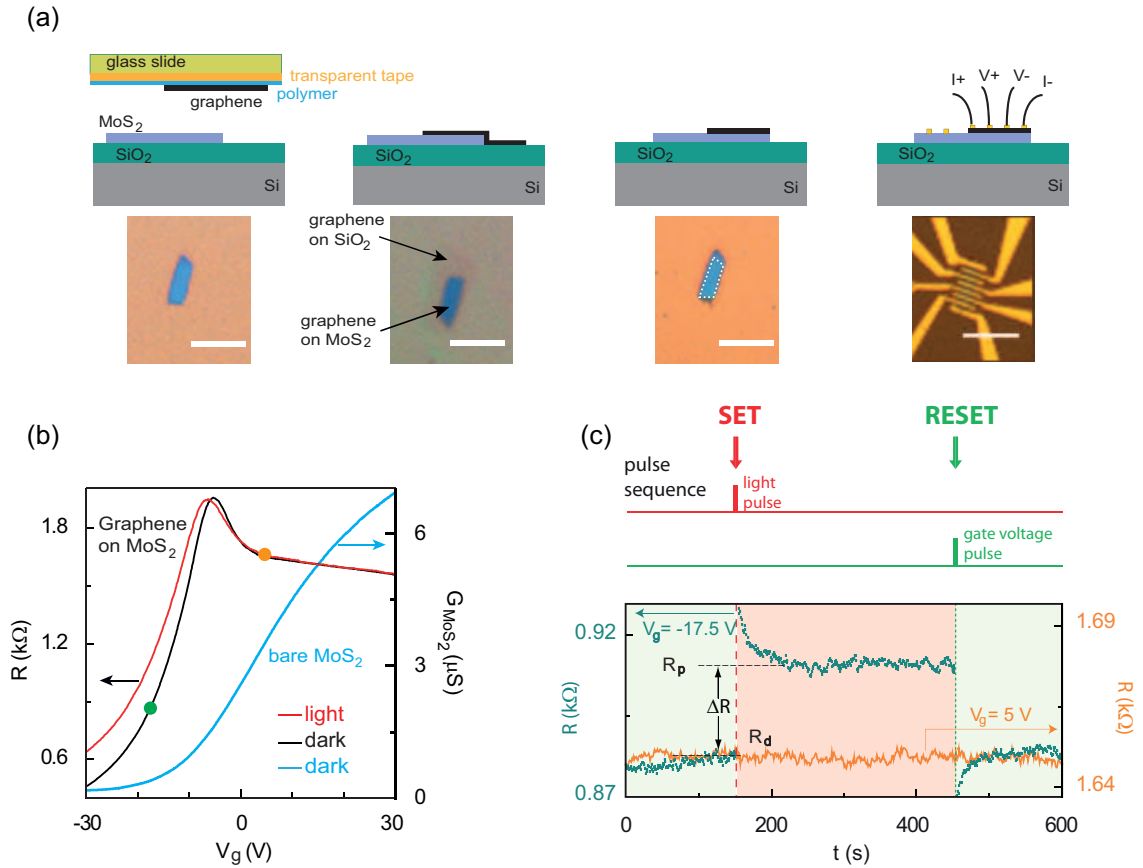


FIG. 1: **Device fabrication and basic optoelectronic response.** (a) Schematic of transfer process with corresponding optical images (scale bars are of $10 \mu\text{m}$ length). The dotted line in the third optical image indicates the outline of graphene. (b) Black and red solid curves represents $R - V_g$ traces for graphene on MoS_2 in the absence and presence of white light respectively. Cyan coloured trace shows V_g dependent conductance of bare MoS_2 measured on a different device in dark. (c) Toggling of the system between two states. R vs t plot is shown illustrating the ‘set’ and ‘reset’ operations achieved by light and gate pulses, respectively. For both curves, $I_{LED} = 5 \text{ mA}$. Note that the transient spikes in R following the gate pulses have been removed throughout the manuscript. The vertical red (dashed) and green (dotted) lines are used to indicate the light and gate pulses, respectively.

gions are shown in Fig. 1b. The $R - V_g$ characteristics of graphene, even in the absence of light (black trace in Fig. 1b), was found to be very different from the usual gate transfer characteristics of graphene on an insulating dielectric such as SiO_2 . The normal ‘bell-shaped’ characteristics are observed only at large negative V_g , whereas for positive V_g , R becomes increasingly insensitive to V_g . This asymmetric $R - V_g$ can be readily understood by referring to the $G_{\text{MoS}_2} - V_g$ characteristics of the underlying MoS_2 (cyan trace). Since we used natural n -type MoS_2 for exfoliation, the MoS_2 channel starts populating only for $V_g \gtrsim V_T$, where V_T is the threshold voltage for conduction. Typically, V_T lies between -10 V to -20 V for most multilayer MoS_2 channels that we have measured [26]. Here, when $V_g > V_T$, MoS_2 turns ‘ON’ (conducting), and screens the gate voltage applied to graphene. Two points need to be noted here: First, for the device presented here, the Dirac point ($V_D = -8 \text{ V}$) lies close to V_T , which is a coincidence, and the two voltage scales can be very different (*e.g.* see Fig. 4a, where

$V_D = +14 \text{ V}$). Second, for $V_g \ll V_T$, where MoS_2 behaves as a (poor) dielectric, it does not form a parallel conducting channel.

We now illuminate the device by forward biasing a white LED with a current I_{LED} . The red trace in Fig. 1b was recorded while the device was illuminated continuously with $I_{LED} = 5 \text{ mA}$ corresponding to a photoexcitation power of $\sim 50 \text{ pW}/\mu\text{m}^2$. Note that there is a pronounced effect only on the negative side of the V_T where an *increase* in R is observed in the presence of light. This negative photoconductivity can be understood as a transfer of the photo-generated electrons inside MoS_2 to graphene under the influence of a negative V_g . Since graphene is hole-doped in this regime, addition of electrons increases R . However, when $V_g \gg V_T$, the bands in MoS_2 stay flat due to its near-metallic nature. This suppresses the transfer of photoexcited carriers from MoS_2 to graphene.

The response of the hybrid was found to be significantly more striking when we used pulsed, instead of con-

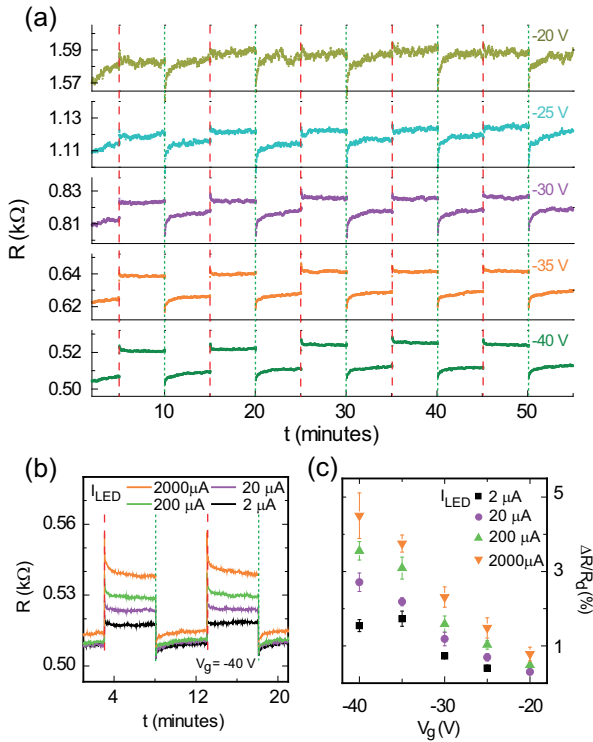


FIG. 2: **Gate and light dependent switching.** (a) The evolution of the switching effect as a function of V_g . For all traces, $I_{LED} = 10 \mu A$. (b) Switching action at different light intensities. (c) Percentage change in resistance as a function of gate voltage calculated from traces similar to those shown in (b).

tinuous, photoexcitation. Fig. 1c shows the response of R to a sequence of light and gate voltage pulses for two different V_g on opposite sides of V_T (denoted by the markers in Fig. 1b). At $V_g = -17.5$ V (i.e., $V_g < V_T$) the light pulse (I_{LED} pulse height = 5 mA, pulse width ~ 0.1 s) induces a transient-like behavior in R . It rises instantaneously from its dark state value (R_d), and then decays over few tens of seconds to a *higher* final value (R_p), indicating a persistent negative photoconductivity. The magnitude of PPC is defined as $\Delta R = R_p - R_d$. On the other hand, it is clear that when $V_g > V_T$ ($V_g = +5$ V), the light pulse has no measurable effect on R , in agreement with experiments performed with continuous illumination. This sensitivity of the PPC to the relative positions of V_g and V_T allowed us to develop a strategy to *erase* the PPC in our devices. By introducing a pulse in V_g we were able to ‘reset’ the device to its original dark state resistance from the persistent state. The trace corresponding to $V_g = -17.5$ V in Fig. 1c demonstrates this switching. A gate voltage of pulse height ΔV and duration ≈ 0.5 s restored R to R_d within a timescale limited by the measurement/pulsing electronics. Typically, we used $\Delta V = +20$ V, so that $V_g + \Delta V \gtrsim V_T$. We would like to point out that our control experiments with MoS₂ and graphene separately show no clear evidence of PPC

in both cases (see Fig. S1 in supplementary information (SI)).

Fig. 2a shows the evolution of the PPC cycles with V_g ($I_{LED} = 10 \mu A$). It is clear that $\Delta R/R_d$ is largest for $V_g = -40$ V, and almost vanishes when V_g is increased to -20 V. At any V_g , the ‘light set - voltage reset’ cycles could be performed over days with better than 95% accuracy in recovering the PPC magnitude. The PPC magnitude also decreases when the intensity of light pulse is reduced, as can be seen in Fig. 2b, where we varied I_{LED} over three decades of magnitude. The results of Figs. 2a and 2b are summarized in Fig. 2c where $\Delta R/R_d$ is plotted as a function of V_g for various light intensities. $\Delta R/R_d$ is found to be as large as 5% at $T \sim 110$ K (similar values of PPC can be achieved at room temperature by making V_g more negative). It is perhaps not surprising that the PPC magnitude depends on the light intensity, however its extreme sensitivity to gate voltage opens up the possibility of creating a new class of electrically tunable optoelectronic devices.

A key feature of the switching cycles in Fig. 2 is the absence of a time-dependent decay in the photoconductivity in the persistent state, particularly at low photoillumination intensity (Fig. 2b). In Fig. 3a we have plotted the photoconductivity in the persistent state in one of the cycles after a low-intensity pulse ($I_{LED} = 2 \mu A$) for three different V_g . The PPC shows no decay with time over three decades irrespective of V_g , remaining essentially constant even when we monitored it over more than 10 hours (inset of Fig. 3b, here $I_{LED} = 5 \mu A$ and $V_g = -40$ V have been used). At higher I_{LED} ($\gtrsim 50 \mu A$), we do observe a logarithmic decay at times < 50 s, although at long times photoconductivity becomes nearly time-independent again. This is illustrated in Fig. 3b with PPC relaxation for $I_{LED} = 200 \mu A$ pulses.

The near-absence of time decay of the persistent state suggests a strong potential barrier that prohibits recombination of electron and holes created on photoillumination. To understand this we note that the majority carriers (electrons) in natural MoS₂ flakes are strongly localized [26], and display Mott-type variable range hopping transport when V_g is reduced to the conduction threshold V_T . Thus our graphene-MoS₂ hybrid behaves as a heterojunction of a doped conducting system (graphene) and a semiconductor (MoS₂) where the carriers are localized, and trapped in potential wells that separate them from the conducting region [16]. V_T represents the gate voltage at which the Fermi energy (E_F) approaches the mobility edge (E_c). The distribution of carriers [16] right after the light pulse ($t = 0$) is shown in the schematic of Fig. 3c. The electrons are swept towards the graphene-MoS₂ interface, and addition of electrons to the p-doped graphene results in an immediate increase in R . The holes remain trapped in MoS₂, but after light is switched off the hole distribution is modified by: (1) quantum tunneling mediated electron-hole recombination, and (2) thermal excitation of holes from the graphene to MoS₂. The PPC then determined by the

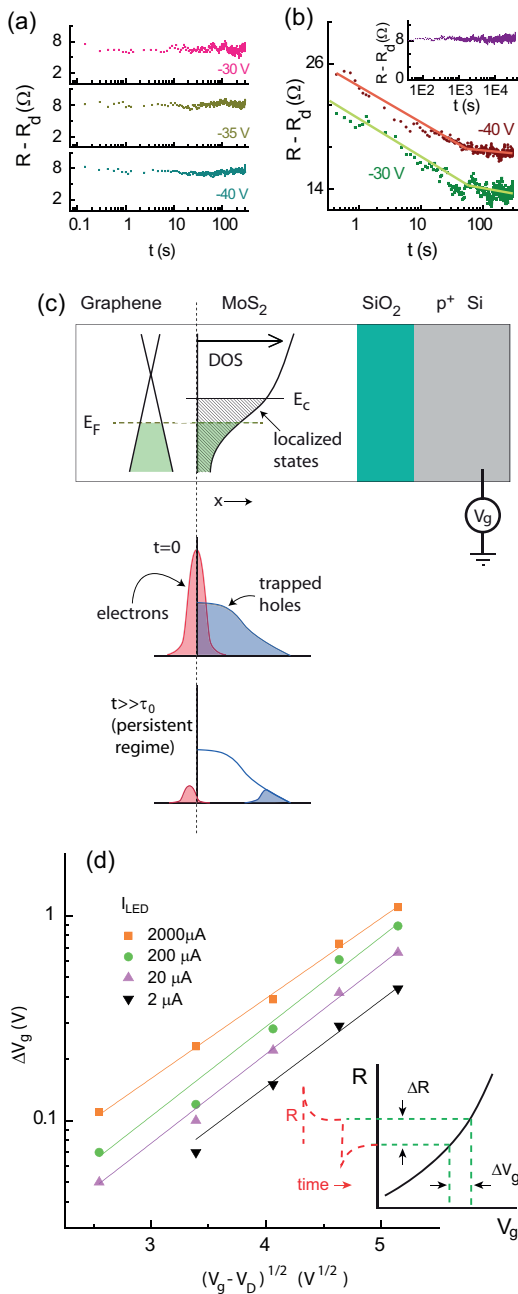


FIG. 3: PPC relaxation nature and mechanism. (a) Nearly relaxation free nature of persistent states at three different gate voltages. $I_{LED} = 2 \mu\text{A}$ has been used for 0.1 s to ‘excite’ the system. (b) Transition from logarithmic decay to nearly relaxation free state after photoexcitation with LED current $200 \mu\text{A}$ for 0.1s. Solid lines are guide to eye. Inset shows the trace of ‘ON’ state over long time scale (~ 12 hrs). (c) Schematic showing the evolution of electron-hole distribution in the system as a function of time. $t = 0$ corresponds to the moment after the light pulse. (d) ΔV_g vs. $\sqrt{V_g - V_D}$. This plot is calculated using the data shown in Fig. 2c. The inset illustrates the conversion of ΔR to ΔV_g .

excess electron density, $n(t)$, left in graphene at time t after the illumination is turned off. As derived in the supplementary information (Eq. S5), $n(t)$ can be expressed as,

$$n(t) \propto f(t) \exp[(E_C - E_F)/k_B T] \quad (1)$$

where $f(t)$ is a logarithmically decaying function when the initial hole distribution is assumed continuous and uniform. However, $f(t) \rightarrow \text{constant}$ for isolated local accumulation of holes far away from the graphene-MoS₂ interface, as the recombination time becomes exponentially long. This is consistent with the observation that decay-free PPC occurs only for weak illumination, or at long time when the illumination is strong. Strong localization in MoS₂ makes recombination via quantum tunneling or thermal activation virtually ineffective, and the equilibrium is restored only by lifting E_F to E_C , which provides the ‘erasing’ mechanism of the PPC as R reverts to its dark-state resistance.

To address the V_g -dependence, we estimated $n(t)$ from the asymptotic time-independent value of ΔR and the equivalent shift (ΔV_g) in the gate voltage. The scheme is shown in the inset of Fig. 3d, where ΔV_g could be evaluated directly from the experimentally measured $R - V_g$ characteristics (black trace in Fig. 1b). Due to the linear bands in graphene (see SI for details), we find:

$$\Delta V_g \propto \exp[\beta \sqrt{|V_g - V_D|}] \quad (2)$$

where $\beta = \hbar v_F \sqrt{(\pi C_{eff}/e)}/k_B T$. Here, C_{eff} is the effective capacitance between the silicon backgate and graphene and v_F is the Fermi velocity in graphene. The exponential increase in ΔV_g with $|V_g - V_D|^{1/2}$ is clearly observed for different photoexcitations in Fig. 3c. Experimentally, we get $\beta \approx 1.1$ which indicates that C_{eff} is about a factor of ~ 5 smaller than the bare capacitance of 285 nm SiO₂ that we used as gate dielectric. This can be readily attributed to the quantum capacitance of the MoS₂ film which acts as a ‘leaky’ capacitor. Note that, if we consider this modified value of the capacitance, we find that the mobility of graphene in our sample is $\sim 12,000 \text{ cm}^2 \text{V}^{-1} \text{s}^{-1}$ which is higher than that typically obtained for exfoliated graphene on bare SiO₂ substrates.

Finally, we ask three important questions: (i) whether the PPC can be observed in other graphene devices, particularly for large area scalability (ii) can the devices work at room temperature, and (iii) how stable are the devices over long-time operation (suitable for non-volatile memory applications).

We have fabricated similar devices by transferring graphene grown via chemical vapor deposition (CVD) onto exfoliated multilayer MoS₂. In the inset of Fig. 4a, we show an optical image of one such device. The $R - V_g$ curves of the device with and without light are shown in Fig. 4a. The CVD-device behaves very similarly to

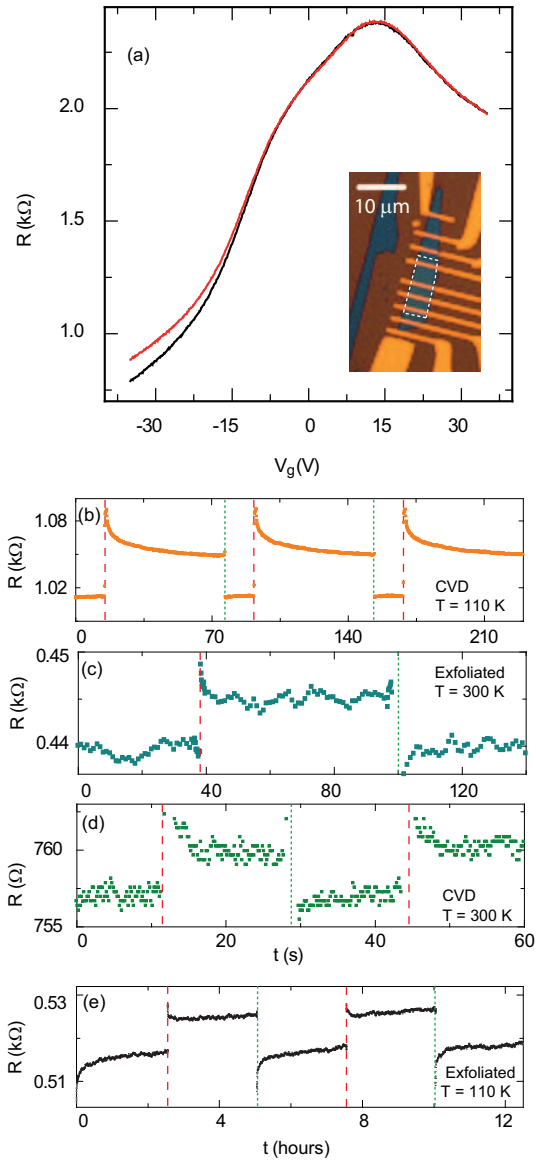


FIG. 4: **Scalability, room-temperature operation and long-term retention.** (a) $R - V_g$ of a device made of CVD-graphene transferred onto exfoliated MoS_2 . Inset: optical image of the device where white dashed line is the guide to the graphene outline. (b) Switching action of the device at 110 K. $V_g = -30$ V and I_{LED} is 5 mA. (c) Data from the exfoliated device at room temperature, $I_{LED} = 5$ mA. (d) CVD device at room temperature, $I_{LED} = 5$ mA (e) Data showing the stability of the system in a timescale of hours. Here, $V_g = -40$ V and $I_{LED} = 5 \mu\text{A}$.

the exfoliated device, albeit with a smaller magnitude of $\Delta R/R_d$ for the same intensity of illumination. This might be correlated with the lower mobility and higher disorder typically associated with CVD growth [27, 28]. Nevertheless, the switching action shown in Fig. 4b confirms PPC. Note that a recent report has shown that large scale CVD growth of MoS_2 is possible on graphene substrates [29], thereby paving new ways for large area device designs.

In Figs. 4c and 4d, we show that PPC is observable even at room temperature for both exfoliated and CVD-graphene devices. However, thermal broadening reduces the threshold for conduction in MoS_2 , which makes the effect clearly observable only at large negative V_g . For example, the data shown in Fig. 4c corresponds to $V_g = -80$ V. Correspondingly, the gate voltage pulse applied $\Delta V (= +40$ V) for recovery was also large. Fig. 4e shows switching cycles in the exfoliated device over a long period of time extending several hours. It confirms that such devices can be promising for nonvolatile memory applications.

I. METHODS

Transfer procedure for laying graphene on MoS_2 : Here we follow a similar procedure to Zomer *et al.* [2]. A piece of glass is covered with a transparent tape and coated with a polymer such as PMMA or EL-9. Graphene is exfoliated onto this substrate. Separately, MoS_2 is transferred to an Si/SiO_2 substrate by standard mechanical exfoliation and placed on the micromanipulator stage of an MJB3 mask aligner with a custom built heater. The graphene flake, now on a transparent substrate, is positioned upside down and aligned with the MoS_2 flake using the microscope of the aligner. The two are brought into contact at an elevated temperature ($T > 100^\circ\text{C}$) as a result of which graphene, along with the polymer is transferred onto MoS_2 . The polymer is later washed off with acetone.

Device fabrication and measurement: Once transferred onto MoS_2 , graphene (exfoliated or CVD-grown) is etched into a desired shape by oxygen plasma. Contacts are drawn using standard e-beam lithography and metallization is done with Ti/Au (15 nm/45 nm) or Cr/Au (15 nm/45 nm). In devices where contacts need to be put on MoS_2 also, we use Au as the contact metal. Measurements are done on graphene using a standard 4-probe lock-in technique. A commercial white LED is used as the light source.

CVD growth: The CVD-graphene reported in this study was synthesized by low-pressure CVD (base pressure of 1 Torr). 25 μm thick copper foils were annealed at 1000 $^\circ\text{C}$ for 5 minutes under a H_2 flow of 50 sccm to reclaim the pure metal surface. CH_4 and H_2 were then introduced at a rate of 35 sccm and 2 sccm for a growth time of 30 s. The reactor was cooled down to room temperature at a cooling rate of 8 $^\circ\text{C}/\text{minute}$ under a 1000 sccm flow of H_2 .

II. ACKNOWLEDGEMENT

We acknowledge the Department of Science and Technology (DST) for a funded project. S.R. acknowledges support under Grant No. SR/S2/CMP-02/2007.

-
- [1] Dean, C. *et al.* Boron nitride substrates for high-quality graphene electronics. *Nature Nanotech.* **5**, 722–726 (2010).
- [2] Zomer, P. J., Dash, S. P., Tombros, N. & van Wees, B. J. A transfer technique for high mobility graphene devices on commercially available hexagonal boron nitride. *Appl. Phys. Lett.* **99**, 232104 (2011).
- [3] Novoselov, K. S. *et al.* A roadmap for graphene. *Nature* **490**, 192–200 (2012).
- [4] Mak, K. F., Lee, C., Hone, J., Shan, J. & Heinz, T. F. Atomically thin MoS₂: A new direct-gap semiconductor. *Phys. Rev. Lett.* **105**, 136805 (2010).
- [5] Xia, F., Mueller, T., Lin, Y.-m., Valdes-Garcia, A. & Avouris, P. Ultrafast graphene photodetector. *Nature Nanotech.* **4**, 839–843 (2009).
- [6] Xia, F. *et al.* Photocurrent imaging and efficient photon detection in a graphene transistor. *Nano Lett.* **9**, 1039–1044 (2009).
- [7] Ghosh, S., Sarker, B. K., Chunder, A., Zhai, L. & Khondaker, S. I. Position dependent photodetector from large area reduced graphene oxide thin films. *Appl. Phys. Lett.* **96**, 163109 (2010).
- [8] Das Sarma, S., Adam, S., Hwang, E. H. & Rossi, E. Electronic transport in two-dimensional graphene. *Rev. Mod. Phys.* **83**, 407–470 (2011).
- [9] Radisavljevic, B., Radenovic, A., Brivio, J., Giacometti, V. & Kis, A. Single-layer MoS₂ transistors. *Nature Nanotech.* **6**, 147150 (2011).
- [10] Late, D. J., Liu, B., Matte, H. S. S. R., Dravid, V. P. & Rao, C. N. R. Hysteresis in single-layer MoS₂ field effect transistors. *ACS Nano* **6**, 5635–5641 (2012).
- [11] Yin, Z. *et al.* Single-layer MoS₂ phototransistors. *ACS Nano* **6**, 74–80 (2012).
- [12] Lee, H. S. *et al.* MoS₂ nanosheet phototransistors with thickness-modulated optical energy gap. *Nano Lett.* **12**, 3695–3700 (2012).
- [13] Radisavljevic, B., Whitwick, M. B. & Kis, A. Integrated circuits and logic operations based on single-layer MoS₂. *ACS Nano* **5**, 9934–9938 (2011).
- [14] Kastalsky, A. & Hwang, J. Study of persistent photoconductivity effect in n-type selectively doped AlGaAs/GaAs heterojunction. *Solid State Commun.* **51**, 317–322 (1984).
- [15] Nathan, M. I. Persistent photoconductivity in AlGaAs/GaAs modulation doped layers and field effect transistors: A review. *Solid-State Electron.* **29**, 167–172 (1986).
- [16] Queisser, H. J. & Theodorou, D. E. Decay kinetics of persistent photoconductivity in semiconductors. *Phys. Rev. B* **33**, 4027–4033 (1986).
- [17] Borghetti, J. *et al.* Optoelectronic switch and memory devices based on polymer-functionalized carbon nanotube transistors. *Adv. Mater.* **18**, 2535–2540 (2006).
- [18] Dawlaty, J. M. *et al.* Measurement of the optical absorption spectra of epitaxial graphene from terahertz to visible. *Appl. Phys. Lett.* **93**, 131905 (2008).
- [19] Nair, R. R. *et al.* Fine structure constant defines visual transparency of graphene. *Science* **320**, 1308 (2008).
- [20] George, P. A. *et al.* Ultrafast optical-pump terahertz-probe spectroscopy of the carrier relaxation and recombination dynamics in epitaxial graphene. *Nano Lett.* **8**, 4248–4251 (2008).
- [21] Urich, A., Unterrainer, K. & Mueller, T. Intrinsic response time of graphene photodetectors. *Nano Lett.* **11**, 2804–2808 (2011).
- [22] Song, J. C. W., Rudner, M. S., Marcus, C. M. & Levitov, L. S. Hot carrier transport and photocurrent response in graphene. *Nano Lett.* **11**, 4688–4692 (2011).
- [23] Gabor, N. M. *et al.* Hot carrier-assisted intrinsic photoresponse in graphene. *Science* **334**, 648–652 (2011).
- [24] Konstantatos, G. *et al.* Hybrid graphene-quantum dot phototransistors with ultrahigh gain. *Nature Nanotech.* **7**, 363–368 (2012).
- [25] Kim, M., Safron, N. S., Huang, C., Arnold, M. S. & Gopalan, P. Light-driven reversible modulation of doping in graphene. *Nano Lett.* **12**, 182–187 (2012).
- [26] Ghatak, S., Pal, A. N. & Ghosh, A. Nature of electronic states in atomically thin MoS₂ field-effect transistors. *ACS Nano* **5**, 7707–7712 (2011).
- [27] Mattevi, C., Kim, H. & Chhowalla, M. A review of chemical vapour deposition of graphene on copper. *J. Mater. Chem.* **21**, 3324–3334 (2011).
- [28] Pal, A. N., Bol, A. A. & Ghosh, A. Large low-frequency resistance noise in chemical vapor deposited graphene. *Appl. Phys. Lett.* **97**, 133504 (2010).
- [29] Shi, Y. *et al.* Van der Waals epitaxy of MoS₂ layers using graphene as growth templates. *Nano Lett.* **12**, 2784–2791 (2012).